Dyes and Pigments 107 (2014) 45–50

Contents lists available at ScienceDirect

Dyes and Pigments

journal homepage: www.elsevier.com/locate/dyepig

A new highly selective and sensitive fluorescent probe for Zn^{2+} and its application in cell-imaging

Quan Hu [a], Yiqun Tan [b], Min Liu [b], Jiancan Yu [b], Yuanjing Cui [b], Yu Yang [b,*]

[a] Department of Pharmacy, School of Medicine, Hangzhou Normal University, Hangzhou 310036, PR China
[b] State Key Laboratory of Silicon Materials, Cyrus Tang Center for Sensor Materials and Applications, Department of Materials Science & Engineering, Zhejiang University, Hangzhou 310027, PR China

ARTICLE INFO

Article history:
Received 5 January 2014
Received in revised form
17 February 2014
Accepted 11 March 2014
Available online 25 March 2014

Keywords:
Chemosensor
Fluorescent probe
Zinc
Fluorescence
Intramolecular charge transfer
Cell-imaging

ABSTRACT

A new fluorescent probe, 3-((4-([2,2′:6′,2″-terpyridin]-4′-yl)phenyl)ethynyl)-7-methoxy-2H-chromen-2-one (ZC-F7) composed of coumarin as the fluorophore and terpyridine as the receptor is designed and synthesized. Based on the intramolecular charge transfer (ICT) effect, the probe exhibits significant variation on emission wavelengths with shifts more than 100 nm after combined with Zn^{2+}, in accordance with the conversion of emission colors from blue to green. Good selectivity and sensitivity of this probe towards Zn^{2+} can be found even on the ppb level in aqueous solution. The Job's plot test suggests a 1:1 stoichiometry between ZC-F7 and Zn^{2+}. The application of the fluorescence probe in bio-imaging is also demonstrated, proving its potential usage in fields such as environment protection, water treatment and safety inspection.

1. Introduction

As the second most abundant transition metal ion in human body, zinc plays an important role in the gene transcription, regulation of metalloenzymes, neural signal transmission and apoptosis [1–5]. Its deficiency causes acrodermatitis enteropathica [6], while excess zinc may also cause serious neurological disorders such as Alzheimer's and Parkinson's diseases [7–9]. It is found that the imbalance in zinc may cause several health problem including superficial skin diseases, prostate cancer, diabetes, and brain diseases [10–12]. Thus, extensive research efforts have been devoted on the quantitative measurement of trace Zn^{2+} in vivo [13–15]. Because of the lack of spectroscopic signature of Zn^{2+}, the method of fluorescent probe has become one of the best choices for detecting and tracking Zn^{2+} in cell-imaging and neurobiological experiments [16].

In recent years, a lot of fluorescent probes for detecting Zn^{2+} have been developed and most of them exhibit good performances in the cellular use [17–27]. However, many fluorescence sensors are still baring problems of selectivity, especially the interruption from Cd^{2+} which possesses very similar chemical properties with Zn^{2+} because of their location at the same group. Recently, Jiang et al. have reported an inspiring distinguishing method for Zn^{2+} and Cd^{2+} by introducing carbonyl group [28,29]. Ng et al. developed two fluorescence sensors for differential detection Zn^{2+} and Cd^{2+} based on BODIPY which can respond towards Zn^{2+} and Cd^{2+} respectively [30]. Nevertheless, reports about the application of these probes in cell-imaging have been barely mentioned.

The development of novel fluorescent probe for metal ions with high sensitivity and selectivity has long been concerned by our group [31–34]. We have developed a new fluorescent probe ZC-F1 based on intra-molecular transfer (ICT) effect for recognizing Zn^{2+} from Cd^{2+} with the detection limit under ppb level [31]. However, it cannot be used in bio-imaging because of two reasons: a) the poor solubility of ZC-F1 in aqueous solution restricts its application in vivo. b) The quantum yield of fluorophores baring ICT effect usually reduces sharply in real practice after the electron withdrawing group combined with metal ions, especially in solvents with high polarity, for the decrease of the energy gap between ground state and excited state [35–38]. To get over these obstacles, a new fluorescent probe highly sensitive and selective towards Zn^{2+} with better solubility and higher quantum yield is required.

Herein, we report a new fluorescent probe 3-((4-([2,2′:6′,2″-terpyridin]-4′-yl)phenyl)ethynyl)-7-methoxy-2H-chromen-2-one (ZC-F7). This probe contains 7-methoxycoumarin, which is known

* Corresponding author. Tel.: +86 571 87952334; fax: +86 571 87951234.
E-mail address: yuyang@zju.edu.cn (Y. Yang).

http://dx.doi.org/10.1016/j.dyepig.2014.03.018
0143-7208/

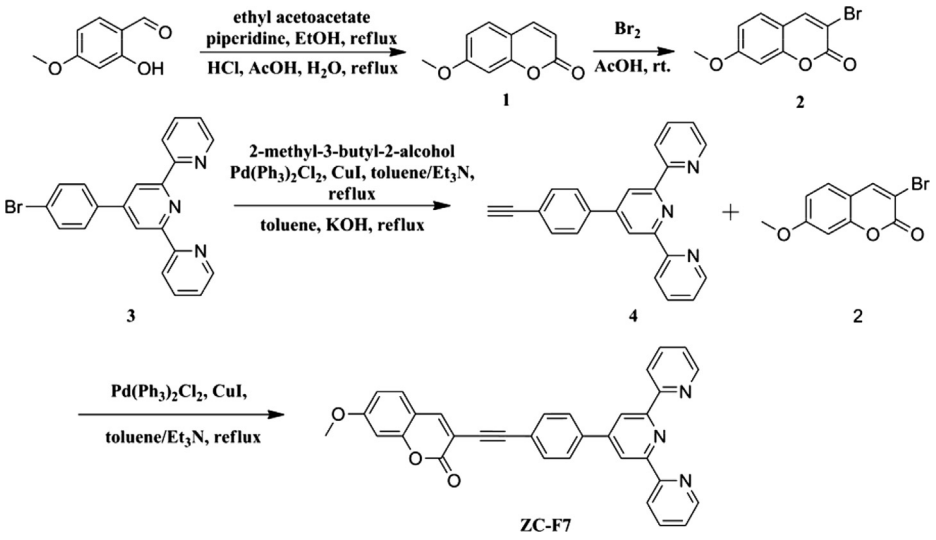

Scheme 1. Synthesis of ZC-F7.

as a water soluble fluorophore and terpyridine as the receptor [39]. To overcome the fluorescence decrease resulted from metal ion binding induced ICT enhancement, the methoxy group is also a good choice as the electron donor, which possess less electron-donating ability than other common donor such like amino group, inducing weaker ICT effect and wider energy gap between ground state and excited state. Thus, after combined with metal ions, the energy gap may not be reduced so sharply and the fluorescence enhancement in aqueous solution can be expected.

2. Experimental section

2.1. Materials and measurements

Solvents and reagents were obtained from commercial source and used as received without further purification. **1** and **2** are synthesized according to literature [40].

^{1}H NMR spectra were recorded in $CDCl_3$ on a 500 MHz Bruker Avance DMX500 spectrometer with tetramethysilane (TMS) as an internal standard. Elemental analysis was performed using a Thermo Finnigan Flash EA1112 microelemental analyzer. Differential scanning calorimetry (DSC) was performed on a Netzsch Instruments 200 F3 at a heating rate of 10 K/min under nitrogen atmosphere. Fluorescence emission spectra and excitation spectra were obtained on a Hitachi F4600 fluorescence spectrophotometer. UV–vis absorption spectra were obtained using a Perkin–Elmer Lambda spectrophotometer. The Fluorescence decay curves were measured by an Edinburgh Instrument F900. Fluorescence quantum yield is measured with integrating sphere on Edinburgh Instrument F900. Fluorescence images were obtained on confocal laser scanning microscopes (CLSM, fluoview FV1000, Olympus).

2.2. Synthesis

2.2.1. 4′-(p-Bromophenyl)-2,2′:6′,2″-terpyridine (**3**)

4-bromobenzaldehyde (1 g, 5.4 mmol) and 2-acetylpyridine (1.3 g, 10.8 mmol) were stirred into methanol (120 mL) followed by addition of NaOH (0.22 g, 5.4 mmol) and NH_4OH 30 mL. The mixture was refluxed for 36 h, and then cooled down to room temperature. The precipitate was filtered and washed by methanol and water to obtain white powder (0.8 g, 40%). ^{1}H NMR (500 MHz, $CDCl_3$): δ = 8.78(t, 4H, J = 12 Hz, ArH) 8.74(d, 2H, J = 7 Hz, ArH) 7.97(s, 2H, ArH), 7.85(d, 2H, J = 8 Hz, ArH), 7.67(d, 2H, J = 2 Hz, ArH), 7.44(s, 2H, ArH); IR(KBr pallet, cm^{-1}): 1605s, 1584s, 1567s, 1541s, 1489s, 1468s, 1443s, 1409s, 1380s, 1074s, 1037s, 1007s, 990s, 888s, 821s, 786s, 733s, 703s, 660s, 627s, 615s, 575s, 497s, 476s, 449s, 420s; MS-ESI theoretical: m/z [M + H]$^+$ = 388.04, found: 388.26; Mp: 137.8 °C; Anal. Calcd for $C_{21}H_{14}BrN_3$: C, 64.96; N, 10.82; H, 3.63. Found: C, 65.03; N, 10.79; H, 3.66.

2.2.2. 4′-(4-ethynylphenyl)-2,2′:6′,2″-terpyridine (**4**)

3 (1.94 g, 5 mmol), $Pd(PPh_3)_2Cl_2$ (0.14 g, 0.2 mmol), 2-methyl-3-butyn-2-ol (1.26 g, 15 mmol) and CuI (0.038 g, 0.2 mmol) were added into a mixture of Et_3N (4 mL) and toluene (16 mL) and refluxed for 12 h. The solution was evaporated and purified by chromatography using CH_2Cl_2 and EtOAC (20:1) as eluent, resulting in white crystal, which is stirred into toluene with KOH (0.56 g, 10 mmol) and refluxed for 2 h. The solution was then extracted with CH_2Cl_2, and the organic phase was combined and evaporated. The resulting black solid was purified by chromatography, using EtOAC and petroleum (1:2) as eluent, afforded pale solid **4** (0.94 g, 48%). ^{1}H NMR (500 MHz, CDCl3): δ = 8.68(t, 4H, J = 7 Hz, ArH), 8.62(d, 2H, J = 8 Hz, ArH), 7.84(m, 4H, J = 8 Hz, ArH), 7.71(d, 2H, J = 8.5 Hz, ArH), 7.32(t, 2H, J = 6 Hz, ArH), 3.11(s, 1H, CH); IR(KBr pallet, cm^{-1}): 3202s, 3063m, 1653w, 1605s, 1585s, 1566s, 1540m, 1510m, 1466s, 1441m, 1412s, 1388m, 1110m, 1076m, 1038m, 990s, 847m, 839s, 825w, 788s, 744m, 734s, 678m, 659m, 623m, 578s, 534m, 516w; MS-ESI theoretical: m/z [M + H]$^+$ = 334.13, found: 334.21; Mp: 142.1 °C; Anal. Calcd for $C_{23}H_{15}N_3$: C, 82.86; N, 12.60; H, 4.54. Found: C, 82.83; N, 12.73; H, 4.64.

Table 1
Linear photophysical properties of ZC-F7 and ZC-F7-Zn.[a]

	$\varepsilon^b \times 10^4$L mol^{-1} cm^{-1}	τ^c, ns	Φ^d, %	λ_{abs}, nm
ZC-F7	6.25	2.85	6.2	385
ZC-F7-Zn	6.42	3.30	13.0	395

[a] All the compounds were dissolved in solvents (water:DMSO = 99:1) at the concentration of 1 × 10^{-6} M.
[b] The molar absorption coefficient of ZC-F7 and ZC-F7-Zn.
[c] The fluorescence lifetime of ZC-F7 and ZC-F7-Zn.
[d] Fluorescence quantum yield of ZC-F7 and ZC-F7-Zn excited at the respective maximum absorption wavelengths.

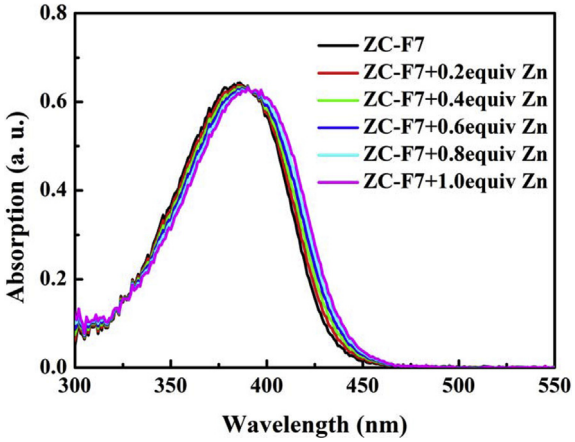

Fig. 1. Absorption spectra of ZC-F7 in DMSO/water (99:1) at 100 nM upon titration of Zn^{2+}.

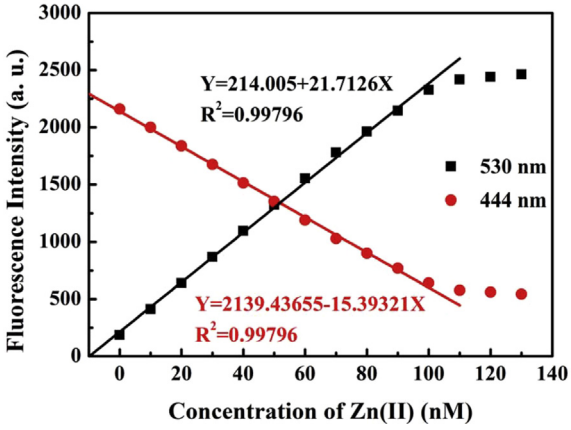

Fig. 3. Fluorescence intensities of ZC-F7 at 444 and 530 nm in the solution with different concentration of Zn^{2+} and their linear fits.

2.2.3. 3-((4-([2,2′:6′,2″-terpyridin]-4′-yl)phenyl)ethynyl)-7-methoxy-2H-chromen-2-one (ZC-F7)

2 (1.01 g, 4 mmol) and **4** (1.32 g, 4 mmol) were solved into a mixture of Et_3N (4 mL) and toluene (16 mL). CuI (0.038 g, 0.2 mmol) and $Pd(PPh_3)_2Cl_2$ (0.14 g, 0.2 mmol) were stirred into the solution and heated at 80 °C for 12 h under argon atmosphere. The resulting solution was evaporated and purified by chromatography using CH_2Cl_2 and petroleum as eluent to yield yellow solid ZC-F7 (1.02 g, 55%). ^1H NMR (500 MHz, $CDCl_3$): $\delta = 8.74$(m, 4H, ArH) 8.68(d, 2H, $J = 8.0$ Hz, ArH) 7.90(m, 5H, ArH), 7.71(d, 2H, $J = 8.5$ Hz, ArH), 7.41(d, 1H, $J = 8.5$ Hz, ArH), 7.36(m, 2H, ArH), 6.89(m, 1H, ArH), 6.85(d, 1H, $J = 2.5$ Hz, ArH), 3.90(s, 3H, CH_3); IR(KBr pallet, cm^{-1}): 3049w, 2925w, 1727s, 1620s, 1600, 1584s, 1565s, 1506s, 1465s, 1440s, 1414m, 1388s, 1364s, 1317m, 1278s, 1226s, 1194w, 1143s, 1121m, 1073w, 1040m, 1016m, 989m, 968m, 917w, 831s, 790s, 767s, 733m, 684m, 660m, 626w, 622w, 575m, 529m; MS-ESI theoretical: m/z $[M + H]^+ = 508.16$, found: 508.23; Mp: 185.3 °C; Anal. Calcd for $C_{33}H_{21}N_3O_3$: C, 78.09; N, 8.28; H, 4.17. Found: C, 78.49; N, 8.32; H, 4.13.

2.3. Cell culture

HeLa human cervical carcinoma cells were cultured in Dulbecco's Modified Eagle's Medium (DMEM, Neuronbc) supplemented with 10% fetal bovine serum (FBS, sijiqing) penicillin (100 units/ml, Boster), and streptomycin (100 μg/mL, Boster). Two days before imaging, the cells were passed and platedon glass-bottomed dishes. For labeling, the growth medium was removed and replaced with DMEM without FBS. The cells were treated and incubated with 10 μL of 1 mM ZC-F7 in DMSO stock solution (10 μM ZC-F7) at 37 °C under 5% CO_2 for 15 min, and provided with 5 μL of fresh media that contained either 1 mM or 0 mM $ZnCl_2$. Then, the cells were incubated for another 15 min at the conditions mentioned above. Prior to imaging, cells were rinsed three times with phosphate buffered saline (PBS).

3. Results and discussion

3.1. Design and synthesis of ZC-F7

In the newly designed fluorescent probe ZC-F7, 7-methoxycoumarin, which is selected as the reporter for its good solubility in water is linked with Zn^{2+} selective receptor terpyridine via ethynyl group as the conjugated bridge. Thus, ICT effect can be expected in this probe. As a promising strategy, intramolecular charge transfer (ICT) was widely used in the design of fluorescent probes [41–44]. Probes based on ICT generally have structures containing an electron withdrawing group conjugated to an electron donating group, which permit ICT from the donor to the acceptor upon excitation, accompany with large Stokes' shift associated with ICT efficiency [45–47]. After combined with metal

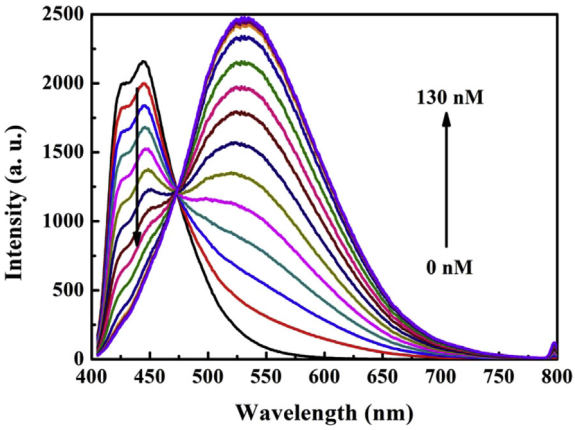

Fig. 2. Fluorescence spectra of ZC-F7 in DMSO/water (99:1) at 100 nM excited at 395 nm upon titration of Zn^{2+}.

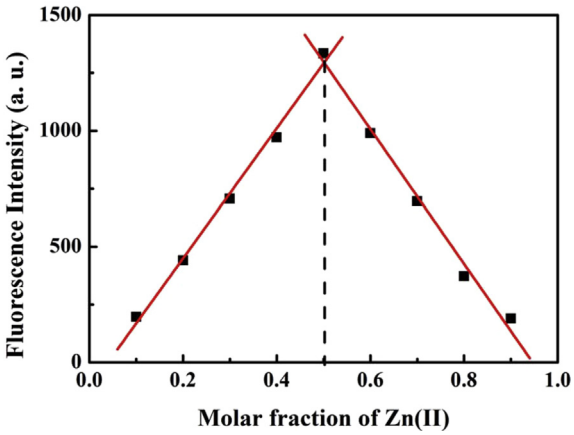

Fig. 4. Job's plot analysis of the stoichiometry of ZC-F7 and Zn^{2+} (excited at 395 nm and monitored at 530 nm).

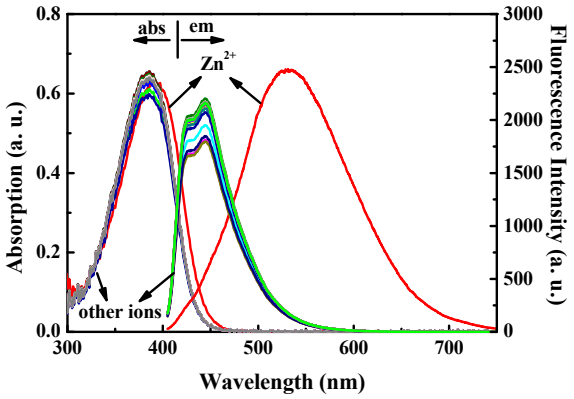

Fig. 5. Absorption and fluorescence emission spectra of ZC-F7 at 100 nM with Ni^{2+}, Cd^{2+},Cr^{3+}, Fe^{3+}, Na^{+}, Ca^{2+}, Pb^{2+}, Al^{3+}, Co^{2+}, Cu^{2+}, Mg^{2+}, K^{+}, F^{-}, Cl^{-}, NO_3^-, PO_4^-, CO_3^{2-} and SCN^{-} upon excitation of 395 nm. The competing ions are at concentration of 100 equiv. (10 μM) and Zn^{2+} is 12 equiv.

ions, the energy level of ICT state is supposed to be reduced, leading to both spectra shift and fluorescence intensity variation [47–50].

As shown in Scheme 1, the compound ZC-F7 can be synthesized in several steps from commercially available chemicals in high yield. Details for synthesis are described in the experiment section. Photophysical parameters of ZC-F7 and ZC-F7-Zn such as quantum yield, fluorescence lifetime, absorption peaks and absorption coefficients are listed in Table 1.

3.2. Optical response of probe ZC-F7

To test the usefulness of ZC-F7 for Zn^{2+} detection, the absorption and fluorescent spectra and its response after titrated with Zn^{2+} are first studied in aqueous solution (water:DMSO = 99:1). With the titration of Zn^{2+}, the absorption peak at 385 nm decreases gradually and a new absorption maximum at 395 nm appears as we can see in Fig. 1. The isosbestic point at 391 nm suggests the complex of Zn^{2+} and the probe. As shown in Fig. 2, a broadband emission spectrum with split peaks located at 425 and 444 nm can be observed. While with the titration of Zn^{2+}, the initial fluorescence bands gradually disappear and a new emission peak at 530 nm owing to the combination of probe and Zn^{2+} is observed. It is worth noting that the fluorescence intensity of ZC-F7 at both 444 nm and 530 nm has well fitted linear relationships with [Zn^{2+}], as we can see in Fig. 3, and significant enhancement of fluorescence intensity can be observed even when [Zn^{2+}] are as low as 10 nM, which equal to 0.65 ppb, indicating that ZC-F7 is highly sensitive for Zn^{2+} even at ppb level. Job's plot is also performed to confirm the possible binding modes of ZC-F1 with Zn^{2+} and certify a 1:1 stoichiometry (Fig. 4).

3.3. Selectivity

To verify the feasibility of ZC-F7 in complicated environment, representative interferences of biological and environmental interests such as Ni^{2+}, Cd^{2+},Cr^{3+}, Fe^{3+}, Na^{+}, Ca^{2+}, Pb^{2+}, Al^{3+}, Co^{2+}, Cu^{2+}, Mg^{2+}, K^{+}, F^{-}, Cl^{-}, NO_3^-, PO_4^-, CO_3^{2-} and SCN^{-} are introduced to investigate their impact on the selectivity of the probe towards Zn^{2+}. As shown in Fig. 5, addition of main group metal ions, including K^{+}, Ca^{2+}, Na^{+}, Mg^{2+} and Al^{3+} exert no influence on the fluorescence intensity before and after treating ZC-F7 with Zn^{2+}, whereas Fe^{3+}, Co^{2+}, Cu^{2+}, Ni^{2+}, Cr^{3+} and Pb^{2+}, quench the fluorescence slightly. Anions such as F^{-}, Cl^{-}, NO_3^-, PO_4^-, CO_3^{2-} and SCN^{-} cause no interruption on the fluorescence spectra of the probe. In addition, Cd^{2+}, as an important disruptor, exhibits little disturbance even at 100 equiv. level, indicating that the probe can tell Zn^{2+} from Cd^{2+} effectively. Moreover, all the interferences mentioned above exhibit almost no influence on the absorption spectra.

3.4. Cell imaging

Taking advantage of the excellent sensing properties for Zn^{2+} in vitro, the assessment whether ZC-F7 can detect Zn^{2+} in live cells

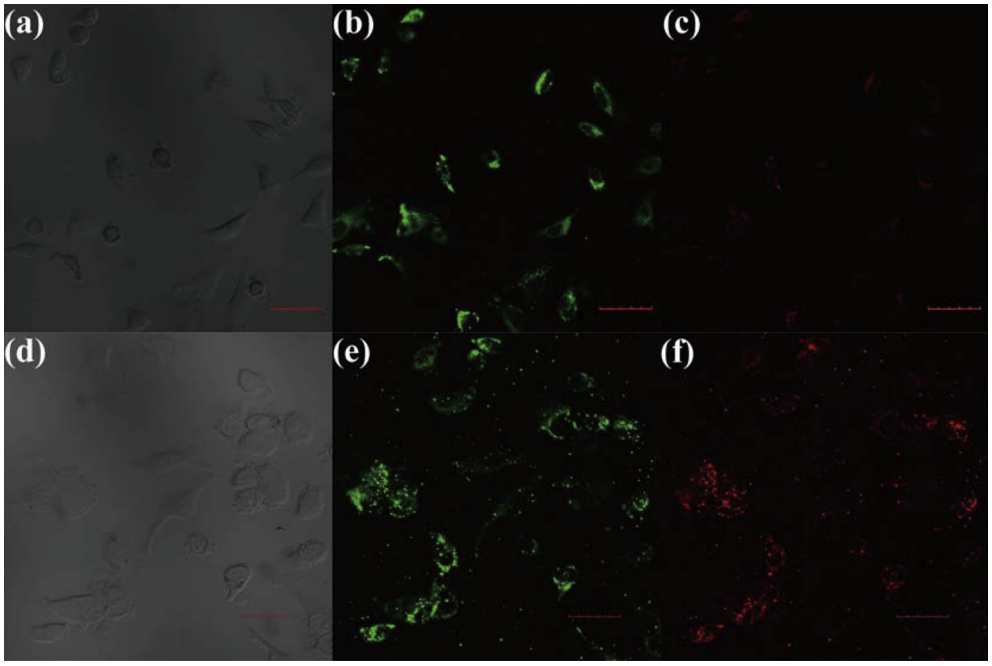

Fig. 6. Images of HeLa cells incubated with ZC-F7 (10 μM) and $ZnCl_2$ at the concentration of 5 μM (a–c) and 0 μM (d–f) for 30 min. Panels (a) and (d) show differential interference contrast (DIC) images, while Panels (b), (c), (e) and (f) show the corresponding confocal fluorescence images collected at 450–530 nm (b and e) and 550–650 nm (c and f). The wavelength for excitation is 405 nm. The scale bar is 50 μm.

is possible by labeling HeLa cells with the probe. As controls, the cells were incubated with 10 μM ZC-F7 for 30 min in DMEM medium at 37 °C, which showed strong intracellular fluorescence in the window of 450–530 nm, while almost no fluorescence can be observed in the detection range of 550–650 nm. Other cells were firstly treated and incubated with 10 μL of 1 mM ZC-F7 in DMSO stock solution (10 μM ZC-F7) at 37 °C under 5% CO_2 for 15 min, and then incubated with DMEM containing $ZnCl_2$ (5 μM) for another 15 min at 37 °C. After incubation, the cells were washed with PBS to remove excess $ZnCl_2$ and the fluorescence in the range of 550–650 nm displayed obviously (excitation at 405 nm) (Fig. 6). The results of the bright-field measurements (Fig. 6(a) and (d)) suggested that the cells were viable throughout the imaging experiments upon treatment with ZC-F7 and Zn^{2+}, respectively. As depicted, these dramatic changes suggested that ZC-F7 was membrane permeable and could response to the presence of Zn^{2+} in live cells. It can be supplied as a useful probe for studying the distribution and physiological activity of Zn^{2+} in live cells.

4. Conclusion

A new fluorescent probe for Zn^{2+} with high sensitivity and selectivity was designed and synthesized and its response was studied. The results showed that the probe can detect Zn^{2+} by two signal channels and minor interruption can be observed from other representative interferences of biological and environmental interests, including Cd^{2+}, which usually plays an important role as a disruptor. This probe exhibited apparent signal change on the ppb level indicating its potential use in the environmental detection of trace Zn^{2+}. In addition, the cell-imaging experiment suggested that ZC-F7 was membrane permeable and could reveal the distribution of Zn^{2+} in live cells. Moreover, these cells were all viable during the experiments, showing a potential usage of ZC-F7 as an indicator for Zn^{2+} in vivo.

Acknowledgment

The authors gratefully acknowledge the financial support for this work from the National Natural Science Foundation of China, China (Nos. 51229201 and 51372221), and Natural Science Foundation of Zhejiang Province (No. LY12E02004).

References

[1] Berg JM, Shi Y. The galvanization of biology: a growing appreciation for the roles of zinc. Science 1996;271(5252):1081–5.
[2] Frederickson CJ, Bush AI. Synaptically released zinc: physiological functions and pathological effects. Biometals 2001;14(3):353–66.
[3] Vallee BL, Falchuk KH. The biochemical basis of zinc physiology. Phys Rev 1993;73(1):79–118.
[4] Voegelin A, Pfister S, Scheinost AC, Marcus MA, Kretzschmar R. Changes in zinc speciation in field soil after contamination with zinc oxide. Environ Sci Technol 2005;39(17):6616–23.
[5] Xie X, Smart TG. A physiological role for endogenous zinc in rat hippocampal synaptic neurotransmission. Nature 1991;349(6309):521–4.
[6] Kury S, Dreno B, Bezieau S, Giraudet S, Kharfi M, Kamoun R, et al. Identification of SLC39A4, a gene involved in acrodermatitis enteropathica. Nat Genet 2002;31(3):239–40.
[7] Cuajungco MP, Lees GJ. Zinc metabolism in the brain: relevance to human neurodegenerative disorders. Neurobiol Dis 1997;4(3–4):137–69.
[8] Bush AI, Pettingell WH, Paradis MD, Tanzi RE. Modulation of A beta adhesiveness and secretase site cleavage by zinc. J Biol Chem 1994;269(16):12152–8.
[9] Koh J-Y, Suh SW, Gwag BJ, He YY, Hsu CY, Choi DW. The role of zinc in selective neuronal death after transient global cerebral ischemia. Science 1996;272(5264):1013–6.
[10] Truong-Tran A, Carter J, Ruffin R, Zalewski P. The role of zinc in caspase activation and apoptotic cell death. Biometals 2001;14(3–4):315–30.
[11] Zalewski PD, Forbes IJ, Seamark RF, Borlinghaus R, Betts WH, Lincoln SF, et al. Flux of intracellular labile zinc during apoptosis (gene-directed cell death) revealed by a specific chemical probe, Zinquin. Chem Biol 1994;1(3):153–61.
[12] Kimura E, Aoki S, Kikuta E, Koike T. A macrocyclic zinc(II) fluorophore as a detector of apoptosis. Proc Natl Acad Sci U S A 2003;100(7):3731–6.
[13] Anthemidis AN, Karapatouchas C-PP. Flow injection on-line hydrophobic sorbent extraction for flame atomic absorption spectrometric determination of cadmium in water samples. Microchim Acta 2008;160(4):455–60.
[14] Davis AC, Calloway Jr CP, Jones BT. Direct determination of cadmium in urine by tungsten-coil inductively coupled plasma atomic emission spectrometry using palladium as a permanent modifier. Talanta 2007;71(3):1144–9.
[15] Kaya G, Yaman M. Online preconcentration for the determination of lead, cadmium and copper by slotted tube atom trap (STAT)-flame atomic absorption spectrometry. Talanta 2008;75(4):1127–33.
[16] Xu Z, Yoon J, Spring DR. Fluorescent chemosensors for Zn^{2+}. Chem Soc Rev 2010;39(6):1996–2006.
[17] Meng X, Wang S, Li Y, Zhu M, Guo Q. 6-Substituted quinoline-based ratiometric two-photon fluorescent probes for biological Zn^{2+} detection. Chem Commun 2012;48(35):4196–8.
[18] Pourghaz Y, Dongare P, Thompson DW, Zhao Y. Click functionalized poly(p-phenylene ethynylene)s as highly selective and sensitive fluorescence turn-on chemosensors for Zn^{2+} and Cd^{2+} ions. Chem Commun 2011;47(39):11014–6.
[19] Sreenath K, Allen JR, Davidson MW, Zhu L. A FRET-based indicator for imaging mitochondrial zinc ions. Chem Commun 2011;47(42):11730–2.
[20] Xu Z, Baek K-H, Kim HN, Cui J, Qian X, Spring DR, et al. Zn^{2+}-triggered amide tautomerization produces a highly Zn^{2+}-selective, cell-permeable, and ratiometric fluorescent sensor. J Am Chem Soc 2009;132(2):601–10.
[21] Baek NY, Heo CH, Lim CS, Masanta G, Cho BR, Kim HM. A highly sensitive two-photon fluorescent probe for mitochondrial zinc ions in living tissue. Chem Commun 2012;48(38):4546–8.
[22] Masanta G, Lim CS, Kim HJ, Han JH, Kim HM, Cho BR. A mitochondrial-targeted two-photon probe for zinc ion. J Am Chem Soc 2011;133(15):5698–700.
[23] Cheng T, Wang T, Zhu W, Chen X, Yang Y, Xu Y, et al. Red-emission fluorescent probe sensing cadmium and pyrophosphate selectively in aqueous solution. Org Lett 2011;13(14):3656–9.
[24] Tian H, Li B, Zhu J, Wang H, Li Y, Xu J, et al. Two selective fluorescent chemosensors for cadmium ions in 99% aqueous solution: the end group effect on the selectivity, DFT calculations and biological applications. Dalt Trans 2012;41(7):2060–5.
[25] Chen X, Shi J, Li Y, Wang F, Wu X, Guo Q, et al. Two-photon fluorescent probes of biological Zn(II) derived from 7-hydroxyquinoline. Org Lett 2009;11(19):4426–9.
[26] Kim HM, Seo MS, An MJ, Hong JH, Tian YS, Choi JH, et al. Two-Photon fluorescent probes for intracellular free zinc ions in living tissue. Angew Chem-Int Ed 2008;47(28):5167–70.
[27] Yin S, Zhang J, Feng H, Zhao Z, Xu L, Qiu H, et al. Zn^{2+}-selective fluorescent turn-on chemosensor based on terpyridine-substituted siloles. Dyes Pigment 2012;95(2):174–9.
[28] Xue L, Liu C, Jiang H. Highly sensitive and selective fluorescent sensor for distinguishing cadmium from zinc ions in aqueous Media. Org Lett 2009;11(7):1655–8.
[29] Xue L, Liu Q, Jiang H. Ratiometric Zn^{2+} fluorescent sensor and new approach for sensing Cd^{2+} by ratiometric displacement. Org Lett 2009;11(15):3454–7.
[30] He H, Ng DK. Differential detection of Zn^{2+} and Cd^{2+} ions by BODIPY-based fluorescent sensors. Chem-Asian J 2013;8(7):1441–6.
[31] Tan Y, Gao J, Yu J, Wang Z, Cui Y, Yang Y, et al. A new fluorescent probe for distinguishing Zn^{2+} and Cd^{2+} with high sensitivity and selectivity. Dalt Trans 2013;42(32):11465–70.
[32] Tan Y, Yu J, Cui Y, Yang Y, Wang Z, Hao X, et al. A novel 2,6-dicarbonylpyridine-based fluorescent chemosensor for Co^{2+} with high selectivity and sensitivity. Analyst 2011;136(24):5283–6.
[33] Tan Y, Yu J, Gao J, Cui Y, Wang Z, Yang Y, et al. A fluorescent pH chemosensor for strongly acidic conditions based on the intramolecular charge transfer (ICT) effect. RSC Adv 2013;3(15):4872–5.
[34] Tan Y, Yu J, Gao J, Cui Y, Yang Y, Qian G. A new fluorescent and colorimetric probe for trace hydrazine with a wide detection range in aqueous solution. Dyes Pigment 2013;99(3):966–71.
[35] Marini A, Munoz-Losa A, Biancardi A, Mennucci B. What is solvatochromism? J Phys Chem B 2010;114(51):17128–35.
[36] Mulliken RS. Molecular compounds and their spectra. III. The interaction of electron donors and acceptors. J Phys Chem 1952;56(7):801–22.
[37] Mulliken RS. Molecular compounds and their spectra. II. J Am Chem Soc 1952;74(3):811–24.
[38] Wu J, Liu W, Ge J, Zhang H, Wang P. New sensing mechanisms for design of fluorescent chemosensors emerging in recent years. Chem Soc Rev 2011;40(7):3483–95.
[39] Jiang Z-J, Lv H-S, Zhu J, Zhao B-X. New fluorescent chemosensor based on quinoline and coumarine for Cu^{2+}. Synth Met 2012;162(23):2112–6.
[40] Simmons JT, Allen JR, Morris DR, Clark RJ, Levenson CW, Davidson MW, et al. Integrated and passive 1,2,3-triazolyl groups in fluorescent indicators for zinc(II) ions: thermodynamic and kinetic evaluations. Inorg Chem 2013;52(10):5838–50.

[41] Kim HM, Cho BR. Two-Photon probes for intracellular free metal ions, acidic vesicles, and lipid rafts in live tissues. Acc Chem Res 2009;42(7):863–72.
[42] Nguyen DM, Frazer A, Rodriguez L, Belfield KD. Selective fluorescence sensing of zinc and mercury ions with hydrophilic 1,2,3-triazolyl fluorene probes. Chem Mater 2010;22(11):3472–81.
[43] Tan Y, Zhang Q, Yu J, Zhao X, Tian Y, Cui Y, et al. Solvent effect on two-photon absorption (TPA) of three novel dyes with large TPA cross-section and red emission. Dyes Pigment 2013;97(1):58–64.
[44] Zhu B, Gao C, Zhao Y, Liu C, Li Y, Wei Q, et al. A 4-hydroxynaphthalimide-derived ratiometric fluorescent chemodosimeter for imaging palladium in living cells. Chem Commun 2011;47(30):8656–8.
[45] Delcamp JH, Shi Y, Yum JH, Sajoto T, Dell'orto E, Barlow S, et al. The role of pi bridges in high-efficiency DSCs based on unsymmetrical squaraines. Chem Eur J 2013;19(5):1819–27.
[46] Karton-Lifshin N, Albertazzi L, Bendikov M, Baran PS, Shabat D. Donor-two-acceptor dye design: a distinct gateway to NIR fluorescence. J Am Chem Soc 2012;134(50):20412–20.
[47] Wu Y-Y, Chen Y, Gou G-Z, Mu W-H, Lv X-J, Du M-L, et al. Large stokes shift induced by intramolecular charge transfer in N,O-chelated naphthyridine–BF2 complexes. Org Lett 2012;14(20):5226–9.
[48] Benniston AC, Winstanley TP, Lemmetyinen H, Tkachenko NV, Harrington RW, Wills C. Large stokes shift fluorescent dyes based on a highly substituted terephthalic acid core. Org Lett 2012;14(6):1374–7.
[49] Poirel A, De Nicola A, Ziessel R. Oligothienyl-bodipys: red and near-infrared emitters. Org Lett 2012;14(22):5696–9.
[50] Rihn S, Retailleau P, De Nicola A, Ulrich G, Ziessel R. Synthetic routes to fluorescent dyes exhibiting large stokes shifts. J Org Chem 2012;77(20):8851–63.